



HAL
open science

Metallo-dielectric metasurfaces for thermal emission with controlled spectral bandwidth and angular aperture

C. Blanchard, L. Wojszvzyk, Cecile Jamois, Jean -Louis Leclercq, Céline Chevalier, Lydie Ferrier, P. Viktorovitch, I. Moldovan-Doyen, François Marquier, Jean-Jacques Greffet, et al.

► To cite this version:

C. Blanchard, L. Wojszvzyk, Cecile Jamois, Jean -Louis Leclercq, Céline Chevalier, et al.. Metallo-dielectric metasurfaces for thermal emission with controlled spectral bandwidth and angular aperture. *Optical Materials Express*, 2022, 12 (1), pp.1-12. 10.1364/OME.443111 . hal-03622069

HAL Id: hal-03622069

<https://hal.science/hal-03622069v1>



Submitted on 4 Apr 2022

HAL is a multi-disciplinary open access archive for the deposit and dissemination of scientific research documents, whether they are published or not. The documents may come from teaching and research institutions in France or abroad, or from public or private research centers.

L'archive ouverte pluridisciplinaire **HAL**, est destinée au dépôt et à la diffusion de documents scientifiques de niveau recherche, publiés ou non, émanant des établissements d'enseignement et de recherche français ou étrangers, des laboratoires publics ou privés.



Metallo-dielectric metasurfaces for thermal emission with controlled spectral bandwidth and angular aperture

CEDRIC BLANCHARD,^{1,4} LEO WOJSZVZYK,² CECILE JAMOIS,³
JEAN-LOUIS LECLERCQ,¹ CELINE CHEVALIER,³ LYDIE FERRIER,³ 
PIERRE VIKTOROVITCH,¹ IOANA MOLDOVAN-DOYEN,² FRANÇOIS
MARQUIER,^{2,5} JEAN-JACQUES GREFFET,²  AND XAVIER
LETARTRE^{1,*} 

¹Université de Lyon, Institut des Nanotechnologies de Lyon, UMR5270 CNRS, Ecole Centrale de Lyon, 69134 Ecully, France

²Laboratoire Charles Fabry, Institut d'Optique, CNRS, Université Paris-Sud, 91127 Palaiseau Cedex, France

³Université de Lyon, Institut des Nanotechnologies de Lyon, UMR5270 CNRS, INSA de Lyon, 7 Avenue Jean Capelle, 69621 Villeurbanne, France

⁴Currently at CNRS, UPR3079 CEMHTI, Univ. Orléans, F-45071 Orléans, France

⁵Currently at Université Paris-Saclay, ENS Paris-Saclay, CNRS, Centrale-Supélec, LuMIn, 91190 Gif-sur-Yvette, France

*xavier.letartre@ec-lyon.fr

Abstract: We introduce thermal metallo-dielectric metasurfaces as mid IR sources. The emitter is a lossy metal. The spectral and angular emission is controlled using a periodic array of high refractive dielectric resonators. We introduce a design that allows to control independently the emission bandwidth and the angular aperture while ensuring a large emissivity. To validate the concept, we fabricated and characterized a metasurface, showing a good agreement with the theory.

© 2021 Optical Society of America under the terms of the [OSA Open Access Publishing Agreement](#)

1. Introduction

One of the simplest ways to produce light is to heat an absorbing material and use its incandescence. An important drawback of incandescence as a source of visible light is the relatively low wall-plug efficiency as most of the heating energy is lost as heat. While this is a major concern for light bulbs, infrared sources can operate in vacuum at temperatures well below the sublimation temperature so that emitters can operate in vacuum and convection losses can be suppressed. As a result, the efficiency can be dominated by radiation losses [1]. The thermal emission produced by homogeneous materials is usually poorly directive and spectrally broad. If a narrow beam and a narrow spectral bandwidth are needed, it is possible to filter spectrally and spatially the emitted signal. This results in a low efficiency source. Tailoring thermal emission so that radiation is emitted only for useful frequencies and directions may result in an efficiency increased by orders of magnitude.

While it has been taken for granted for a long time that incandescent sources were deemed to produce broadband light (temporally incoherent), and poorly directional light (spatially incoherent), it is now understood that it is possible to engineer the spectral and directional emissivity of a source. The purpose of this paper is to introduce a metallodielectric metasurface that provides several degrees of freedom enabling to design a source emitting with emissivity close to 1 at normal incidence with a controlled angular aperture, at a specified wavelength with a controlled spectral bandwidth.

The control of directivity of transmitted and reflected beams by metasurfaces consisting in an array of resonant scatterers is based on interferences of the incident spatially coherent beam by the scatterers. Using metasurfaces for thermal emission is very different as there is no incident coherent beam. Instead, radiation is produced by thermally induced and spatially uncorrelated random currents in the material. However, spatial coherence may emerge from the excitation by the thermal currents of spatially extended modes propagating along the interface. The induced currents associated with these extended modes are then able to produce directional emission patterns. This has been demonstrated using surface phonon polaritons propagating along a SiC surface [2]. Other modes can be used to control directivity such as surface plasmons [3,4]. It has been proposed recently to use delocalized modes in an array of high index resonators [5]. An alternative approach explored theoretically [6] and experimentally [7] is to deposit angle selective multilayers on the emitter to tailor the transmission factor as a function of the emission angle. Beaming has been reported using bull's eyes [8] and two-dimensional scatterers arrays with aperture angles as small as 1° [9] or as large as 30° [10]. More recently, focused emission has been reported [11–13].

The control of the emission spectrum can be achieved using surface waves and operating at the frequency where the dispersion relation has a flat asymptote [14] or using Tamm Plasmon modes [15]. Other possibilities rely in taking advantage of the absorption spectrum of a specific material embedded in a transparent material [16–19]. A more flexible approach is to use an array of resonators controlling the absorption in a lossy material. Many demonstrations were reported using metal-insulator-metal (MIM) resonators [20–23] or resonant cavities [24]. The emission spectrum can also be controlled using dielectric coatings [25,26] or photonic crystals [27–31].

Reviews of early work can be found in [32,33]. Recent reviews [34] also cover important recent topics which are beyond the scope of this paper such as the design of emitters for thermo-photovoltaics applications [18], the design of sources emitting circular polarization or light with orbital angular momentum, and the development of non-reciprocal emitters.

In order to design a thermal emitter with controlled emission spectrum and angular pattern, we need a model of the emission by a structure. According to Kirchhoff's law, engineering the emissivity amounts to engineer the absorptivity. While the original derivation of Kirchhoff used ray optics and was based on the hypothesis that energy reflection factors obey reciprocity, it has been proven in the frame work of wave fields that this assumption is valid for any reciprocal medium [35–37]. We can thus use the tools of coherent nanophotonics to optimize the absorption of an absorbing structure.

In this paper we introduce a method to design a thermal metasurface with an emissivity on the order of one in the normal direction and at a given frequency in the mid infrared. Importantly, we aim at controlling the angular aperture and the spectral bandwidth while using materials that can sustain high temperatures over long periods. We consider a metallo-dielectric system. It will be shown that this strategy allows for the control of the spectral (section 2) and spatial (section 3) coherence of the source independently. An experimental implementation will be presented in section 4.

2. Versatile spectrally selective/coherent thermal emitters

2.1. Metallo-dielectric metasurface

The thermal metasurface consists in a metallic plate made of platinum and a high index dielectric metasurface located in the near-field of the substrate (see Fig. 1).

To optimize the emissivity ε of the source in a given direction (θ_0) and at a given wavelength (λ_0), we couple a resonant structure to a lossy metallic plate with low emissivity. The absorptivity is mostly due to losses in the metal which can be adjusted by tuning the thickness H_{SiO_2} . The emissivity of the device at (λ_0, θ_0) will be maximum ($\varepsilon=1$) if the lifetime of photons into the resonator is equally determined by the absorption of the metal (associated with a lifetime τ_{abs})

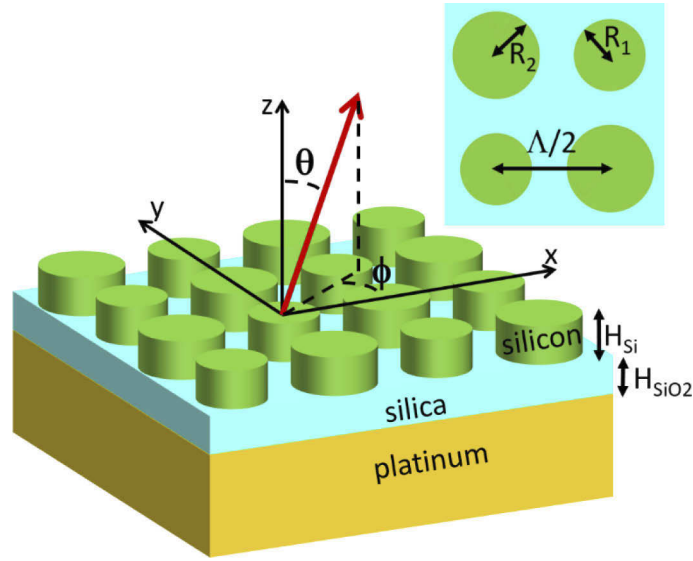


Fig. 1. 3D and top view of the metasurface, defining its geometrical parameters as well as the incident (θ) and azimuthal (ϕ) angles.

and by the scattering of photons in the direction θ_0 (lifetime τ_{opt}). This is the so-called critical coupling condition: $\tau_{abs} = \tau_{opt}$. In that situation, an incident plane wave at wavelength λ_0 , impinging on the device in the direction θ_0 , is fully absorbed. According to Kirchhoff's law, the emissivity is equal to one. Generally speaking, the resonance bandwidth, inversely proportional to the photon lifetime, is given by:

$$\Delta\lambda = \frac{\lambda_0^2}{2\pi c} (1/\tau_{abs} + 1/\tau_{opt})$$

This expression can be written in terms of quality factors:

$$Q_{total}^{-1} = \frac{\Delta\lambda}{\lambda_0} = Q_{abs}^{-1} + Q_{opt}^{-1} \quad (1)$$

Using the coupled modes theory, the emissivity can also be cast in the form [5]:

$$\varepsilon = \frac{4Q_{abs}Q_{opt}}{(Q_{abs} + Q_{opt})^2} \quad (2)$$

which is indeed equal to one if $Q_{abs} = Q_{opt}$. In summary, satisfying the critical coupling condition ensures a maximum emissivity.

2.2. Spectral control

In this work the resonance is provided by the periodic metasurface which is a 2D Photonic Crystal membrane (2D PCM). The device consists in a square lattice of high index dielectric (silicon) micro-pillars deposited onto a metallic plate, separated by a low index spacer (silica). This periodic structure supports guided mode resonances [38] whose optical properties are governed by its geometrical parameters. The losses take place in the metal so that they depend on the permittivity of the metal. More importantly, the absorption depends on the thickness separating the metal from the resonant dielectric structures so that the structure provides a design parameter

to control Q_{abs} . In order to satisfy the critical coupling condition, we need a parameter to control the radiative losses Q_{opt} . As shown on Fig. 1, the elementary cell of the 2D PCM is composed of pillars with two different radii. If $R_1=R_2$, the period is $\Lambda/2$ and is chosen smaller than half the wavelength so that the electromagnetic field of the Bloch mode contains only evanescent waves. In other words, the mode lies below the light line and cannot interact with free space modes so that $\tau_{opt} = \infty$. If however, we introduce a difference between the radii, the period becomes Λ . This leads to a folding in Brillouin zone of this mode above the light line (e.g. at Γ point), allowing the off-plane emission [39]. This periodic modulation of the radii can be seen as a perturbative grating which couples the Bloch mode with free space. This way of controlling the interaction between the resonant and propagating modes is based on breaking a translational invariance. It is very similar to the use of Quasi Bound states In the Continuum (QBIC) introduced in [5].

As a first illustration, a PCM is designed in order to produce thermal emission in the vertical direction at a wavelength around $4.35\mu\text{m}$. To get the spectral emissivity, the absorption is calculated using RCWA (Rigorous Coupling Wave Analysis) simulations [41], for a plane wave at normal incidence. The refractive index of silicon (3.45) and silica (1.4) can be assumed constant in this wavelength range, the optical properties of Platinum are given by Palik's data. To exemplified the concept of critical coupling, the simulated optical properties of the structure (for $\Lambda=4.4\mu\text{m}$, $H_{Si}=0.5\mu\text{m}$, $H_{SiO_2}=0.2\mu\text{m}$) are presented on Fig. 2 for different values of the radii R_1 and R_2 . Two geometrical parameters can be defined which are particularly relevant for controlling the emission properties:

- The global silicon filling factor:

$$FF = \frac{2\pi}{\Lambda^2}(R_1^2 + R_2^2)$$

- The silicon filling factor deviation which is used to control τ_{opt} :

$$\delta FF = \frac{2\pi}{\Lambda^2}(R_2^2 - R_1^2)$$

The spectral emissivity has been calculated for increasing values of δFF . As shown on Fig. 2(a), keeping Λ , FF , H_{Si} and H_{SiO_2} constant produces a resonant wavelength close to $4.35\mu\text{m}$. When $\delta FF=0$ ($R_2=R_1$), the actual period of the structure is $\Lambda/2$ and the resonant mode lies below the light line (at the first edge of the Brillouin zone), resulting in the absence of out coupling of the resonant mode. From this point, increasing δFF leads to a larger coupling and the absorption peak is broader and broader (see Fig. 2(a)). A nearly full absorption is observed (Fig. 2(b)) when $R_1=0.6\mu\text{m}$ and $R_2=0.7\mu\text{m}$ ($\delta FF \sim 0.042$), indicating that the structure is close to the critical coupling condition. On Fig. 2(c), the total quality factor is obtained through the width of the peaks at half maximum when Q_{abs} and Q_{opt} are calculated using Eqs. (1) and (2). It can be pointed out that, when the critical coupling occurs ($\epsilon=1$), Q_{total} is approximately half the one for $R_2=R_1$, which confirms that, at this point, $\tau_{abs} = \tau_{opt}$. Moreover it can be observed that Q_{abs} is nearly constant with δFF . To summarize, with this first design, an efficient ($\epsilon=1$) and partially temporally coherent thermal emission could be obtained at $4.35\mu\text{m}$ with a bandwidth (at half maximum) of 140nm .

At critical coupling, the bandwidth, which is only determined by the absorption rate ($1/\tau_{abs}$), will be strongly affected by the thickness (H_{SiO_2}) of the spacer which governs the interaction between the PCM mode and the absorbing metallic plate. In Fig. 3, we show that a bandwidth varying from 55 to 190nm is obtained when varying H_{SiO_2} from 100 to 500nm . The other parameters are slightly adjusted to maintain the critical coupling condition at the same λ (see table 1).

We note that a related design was proposed in Ref. [5] assuming the metal to be a perfect electric conducting ground plane and controlling the absorption by tuning the silicon doping.

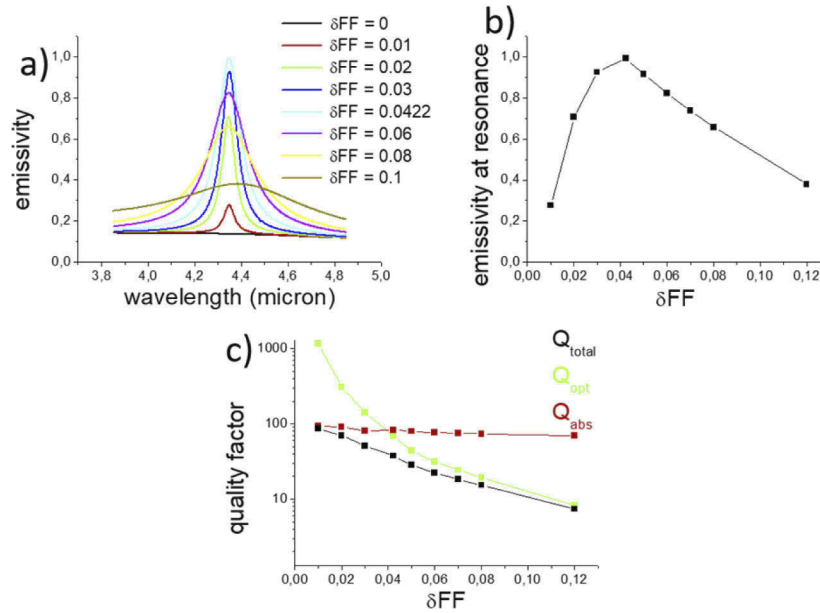


Fig. 2. effect of the filling factor deviation δFF on the spectral properties of the thermal source (the filling factor $FF=0.275$ is kept constant).

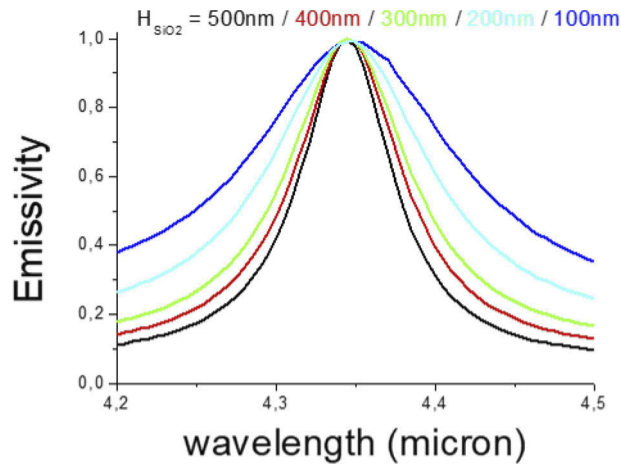


Fig. 3. Effect of the spacer thickness on the spectral bandwidth of the source.

Table 1. geometrical parameters used in Fig. 3 (H_{Si} is kept constant at 500nm)

H_{SiO_2} (nm)	Λ (μm)	R_1 (μm)	R_2 (μm)	λ (μm)	$\Delta\lambda$ (nm)
100	4.2	0.59	0.68	4.35	190
200	4.4	0.6	0.7	4.35	140
300	4.38	0.605	0.705	4.35	100
400	4.43	0.595	0.7	4.35	85
500	4.39	0.59	0.705	4.35	55

Here, we account for the absorption of a real metal and use the resonator-metal distance as a design parameter so that there is no need to control silicon doping.

We now show that it is possible to control the emission frequency by tuning the period of the array. On Fig. 4, the absorption spectra for increasing period (Λ) are presented. For all curves, the stack is identical (same H_{Si} and H_{SiO_2}) and the radii R_1 and R_2 are adjusted to keep FF (~ 0.275) and δFF (~ 0.04) constants. It is observed that the critical coupling condition is preserved for a large range of wavelength peaks. This result gives a simple way to design, on the same stack, a multispectral coherent thermal sources. As an example, the peak wavelength of the orange and black curves on Fig. 4 correspond to the footprints of CO_2 and NO_2 at, respectively, 4.25 and 6.23 μm , indicating that such a source can be used for gas detection of several gas in parallel.

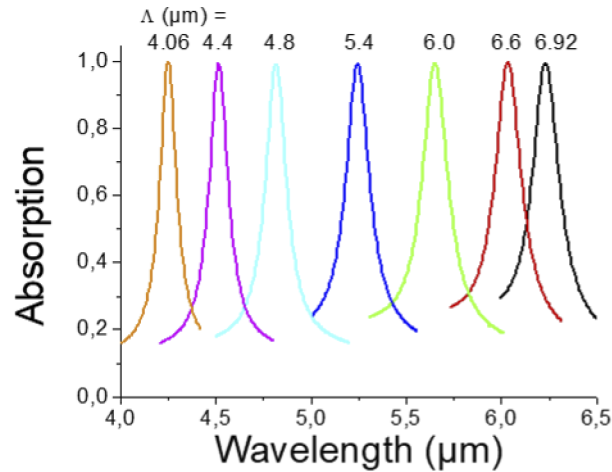


Fig. 4. Effect of the period on the central wavelength of the source (H_{Si} , H_{SiO_2} , FF and δFF constant).

To conclude this section, the association of a metallic plate with a dielectric resonant metasurface offers the possibility to achieve total absorption at normal incidence while controlling independently not only the emission wavelength but also the bandwidth of the source. The ability to control the bandwidth is an advantage as compared to MIM resonators where τ_{abs} depends almost solely on the choice of the metal [20–23].

3. Controlling the spatial coherence to design directional emitters

In this section we address the issue of controlling the angular aperture of the emission around the normal incidence. Since the emission is mediated by the modes of the system, the angular aperture of the emission depends on the structure of the dispersion relation close to $k=0$. More specifically, given a spectral width of the mode corresponding to its coherence time $\tau = \frac{\lambda Q_{total}}{2\pi c}$, the corresponding width Δk can be derived. This interval is inversely proportional to the coherence length L_c . In other words L_c , is the in-plane propagation length of photons during their lifetime in the resonant mode. By assuming a parabolic dispersion relation with curvature b , it was shown [5,40] that the coherence length L_c is given by:

$$L_c \sim \sqrt{b\tau} \quad (3)$$

It should be noted that Eq. (3) was derived assuming that the lifetime τ does not depend on the parallel wave vector (or associated incident angle) or, in other words, that all the modes along a branch of the dispersion relation have the same decay rate. This is not generally the case so that the simplified coupled mode theory has to be replaced by an exact numerical simulation.

Let us focus on a nominal structure defined by the parameters indicated in red in table 1. On Fig. 5, the calculated emissivity as a function of wavelength and incident angle is presented for different polarization and azimuthal angle (see Fig. 1 for definitions). As reminded in the previous section, a large emissivity requires a balance between absorption and radiative losses. When increasing the incident angle, the coupling of the mode with free-space is modified and the critical coupling condition is no longer fulfilled so that the emissivity drops. This provides a means to control the angular aperture of the emitter. It turns out that the modification of the coupling of the mode to free space can occur through two different mechanisms as explained in the following:

- On Fig. 5(a) (p polarization, 0° azimuthal angle), a progressive decreasing of the peak emissivity with the incident angle is observed. It is due to a decreasing coupling to free space, $\frac{1}{\tau_{opt}}$, as a function of the angle. It has to be noticed that this coupling occurs only with the zero-order diffractive free-space mode.
- The situation is drastically different in Fig. 5(b) (s polarization, 45° azimuthal angle). Indeed, for an incident angle of about 25° , the mode crosses the limit for first-order diffraction (dashed black line). It means that, beyond this point, it can couple to an additional radiative loss channel so that the critical coupling condition is no longer fulfilled. As a consequence, there is an abrupt drop of the emissivity in the zero-order diffractive mode. The angle where this modification occurs can be tuned by controlling the periodicity of the surface. This behavior has been also used to tune the angular aperture of metasurfaces made with metallic MIM resonators [10].

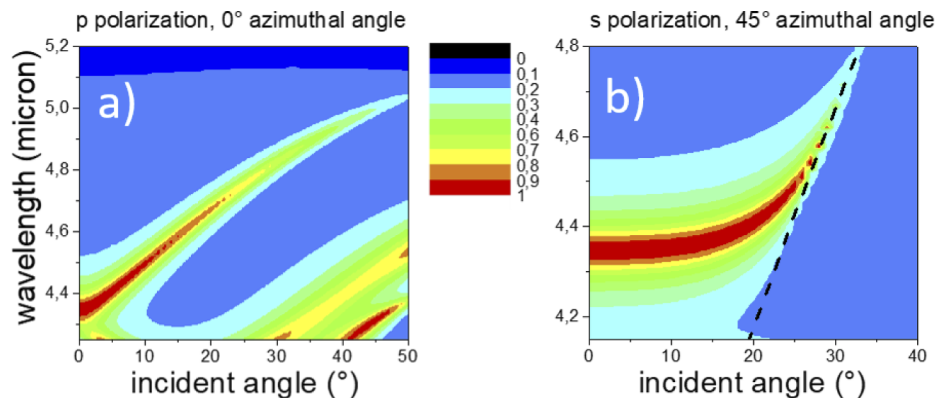


Fig. 5. emissivity maps a) for p polarization and 0° azimuthal angle and b) for s polarization and 45° azimuthal angle. Below the dashed black line the first order diffraction order appears.

The total emissivity of the structure will be obtained by an averaging over all polarizations and azimuthal angles. Therefore, both processes described above will participate to the angular selectivity (or spatial coherence) of the thermal source.

4. Experimental demonstration

A dielectric metasurface has been fabricated (Fig. 6) which is composed of an array of silicon pillars separated from a platinum plate by a silica layer. The metasurface was realized using UV laser direct lithography, followed by a combined CHF₃-based reactive ion etching (RIE) and Cl₂-based inductive coupled plasma (ICP) transfer. In order to obtain the material stack, 400 nm of Pt were deposited by e-beam on a Si (001) undoped substrate. Then 240 nm of SiO₂ spacer

layer, 490 nm of amorphous silicon and 120 nm of Silica hard mask layer were successively deposited by plasma enhanced chemical vapor deposition (PECVD) at 13,56 MHz. The UV lithography process used a double period-based plots pattern arranged in $5 \times 5 \text{ cm}^2$ total surface.

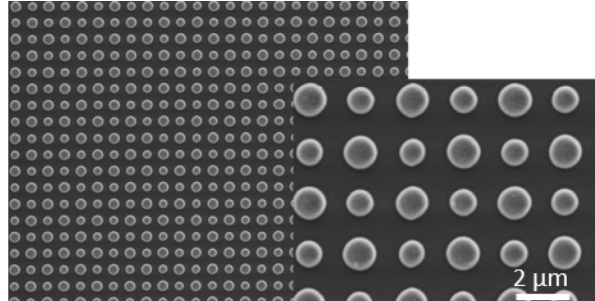


Fig. 6. SEM micrographs of the fabricated metasurface.

As can be seen on the SEM images shown in Fig. 6, the PCM structures obtained by direct laser writing have well-defined features arranged in the desired double period with alternating radius. The geometrical parameters have been measured using a Tescan FEG-SEM. The fabricated pillar arrays show a good homogeneity with a variation of dimensions as low as 2% over their $5 \times 5 \text{ mm}^2$ surface. The average parameters of the experimental PCM have been deduced from statistical analysis of the SEM observations and are 625 nm, 770 nm and $2.30 \mu\text{m}$ for the two radii and the half-period, respectively.

We measured the emissivity by heating the sample at 500°C (773K) on a holder which is fixed on a motorized rotating goniometer. The emitted thermal radiation is collected with a mirror system and sent into a Bruker FTIR spectrometer. We normalize the data by replacing the sample by a calibrated blackbody (SR 200 ECI system) in order to get the emissivity. The setup provides a direct measurement of the emissivity with an angular resolution of 0.5° . More information on the experimental setup can be found in [42].

The measured emissivity is depicted on Fig. 7 as a function of angle and wavelength for both polarizations (s and p) and for the 2 main azimuthal angles (0° and 45°). The resulting maps (center column of Fig. 7) are compared with calculations (left column of Fig. 7). The agreement is qualitatively good, showing maximum signal for wavelength around $4.5 \mu\text{m}$ and predominantly for incident angles between 0 and 20° . The observed discrepancies can be attributed to uncertainties about the refractive index of the materials. We have not characterized the refractive index in situ but used values for crystalline silicon from Palik at ambient temperature. On one hand, the refractive index of deposited materials may depend on the deposition conditions. On the other hand, it depends on the temperature, particularly for the losses of amorphous silicon. The a priori knowledge of these parameters is therefore not within our reach. The optical parameters of the silicon have then been adjusted to better reproduce the measurements (right column in Fig. 7). The comparison is clearly better in terms of resonance wavelength and background absorption. The resulting refractive index of silicon is:

$$\hat{n} = n_0 + i\kappa = 3.53 + 0.03i$$

These values are consistent with the literature as (i) $n_0 = 3.53$ is obtained using the temperature-dependent model given in [43], and (ii) $\kappa = 0.03$ is of the same order of magnitude as those reported in [44] where such a large absorption is attributed to vibrational modes in amorphous silicon. It is interesting to note that the use of other materials and deposition processes (e.g. crystalline silicon) could allow a strong reduction of this background absorption, which would be necessary for the design of thermal sources with a narrower spectral bandwidth.

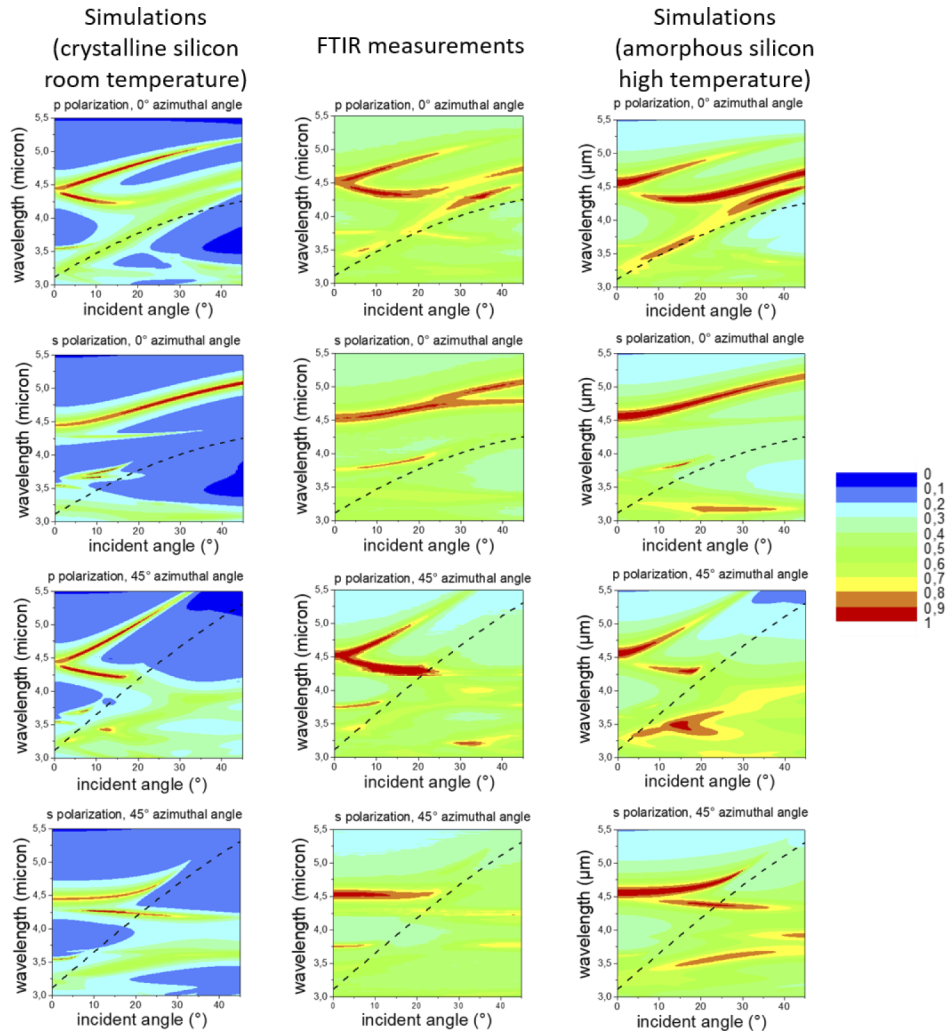


Fig. 7. experimental (center) and simulated (left and right) emissivity maps for different polarization and azimuthal angles (the dashed black line the first order diffraction limit).

The emissivity of the fabricated thermal emitter averaged over the 2 azimuthal angles (0° and 45°) and over the 2 polarizations (p and s) is plotted on Fig. 8. Additional simulations show that this mapping is very close to that obtained by integrating over all azimuthal angles. The following figures can then be calculated considering a useful signal in the 4.4-4.65 μm window and for an angular aperture of 10° :

- The mean emissivity is 80%
- The useful emitted power is 18 times that of a simple platinum plate for the same temperature (500°C).

To conclude this section, these experimental results confirm that a metallo-dielectric metasurface can be used to optimize the thermal emission in a controlled spectral bandwidth and angular aperture around the normal.

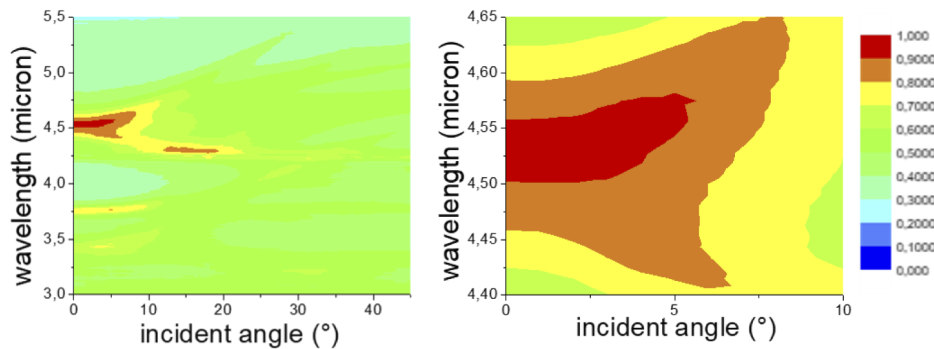


Fig. 8. Experimental averaged emissivity maps. The left map is a zoom on the useful window.

5. Summary

In summary, we have introduced a metallo-dielectric metasurface for thermal emission at normal incidence. The structure takes advantage of the physics of the modes of metasurfaces to provide independent parameters to control the central emission frequency (the period of the metasurface), the spectral bandwidth (the spacing between the metallic substrate and the dielectric resonators), the emissivity (in order to fulfill the critical coupling condition, radiative losses are finely tuned by breaking the translational invariance of the system) and the angular aperture (mainly the period of the metasurface). The design reported in this article is simpler than previous theoretical proposals [5]. It led to the fabrication of a robust sample made with silicon, silica and platinum which can sustain high temperatures. The measurements demonstrate the possibility to control the emissivity.

This method introduces a family of metasurfaces compatible with standard fabrication techniques that can be used to design emitters in the mid IR and operate reliably at 800 K. As compared with previous works where the emitting material (metal [10] or absorbing dielectric [5]) is embedded in the metastructure, the interaction between the absorbing metal and the optical resonance (lying in the dielectric) can be finely adjusted. As a consequence, this family of metallo-dielectric metasurfaces has the potential to design emitters with a full control of the spectral lines (e.g. much narrower). This could be useful to increase the number of independent emission lines for gas sensing. We note that the reduced signal associated with the smaller linewidth can be compensated by increasing the emitting area size.

Funding. Direction Générale de l'Armement; Agence Nationale de la Recherche (ANR-12-NANO-0005, ANR-17-CE24-016).

Disclosures. The authors declare no conflicts of interest

Data availability. Data underlying the results presented in this paper are not publicly available at this time but may be obtained from the authors upon reasonable request.

References

1. G. Brucoli, P. Bouchon, R. Haidar, M. Besbes, H. Benisty, and J.J. Greffet, "High efficiency quasi-monochromatic infra red emitter," *Appl. Phys. Lett.* **104**(8), 081101 (2014).
2. J.J. Greffet, R. Carminati, K. Joulain, J.P. Mulet, S. Mainguy, and Y. Chen, "Coherent emission of light by thermal sources," *Nature* **416**(6876), 61–64 (2002).
3. M. Kreiter, J. Ostens, R. Sambles, S. Herminghaus, S. Mittler-Neher, and W. Knoll, "Thermally induced emission of light from a metallic diffraction grating, mediated by surface plasmons," *Opt. Commun.* **168**(1-4), 117–122 (1999).
4. M. Laroche, F. Marquier, C. Arnold, R. Carminati, J.J. Greffet, S. Collin, N. Bardou, and J.L. Pelouard, "Highly directional radiation generated by a tungsten thermal source," *Opt. Lett.* **30**(19), 2623 (2005).
5. A. C. Overvig, S. A. Mann, and A. Alù, "Thermal metasurfaces: complete emission control by combining local and nonlocal light-matter interactions," *Phys.Rev.X* **11**, 021050 (2021).

6. J. Drevillon and P. Ben-Abdallah, "Ab initio design of coherent thermal sources," *J. Appl. Phys.* **102**(11), 114305 (2007).
7. B. J. Lee and Z. M. Zhang, "Design and fabrication of planar multilayer structures with coherent thermal emission characteristics," *J. Appl. Phys.* **100**(6), 063529 (2006).
8. S. Han and D. Norris, "Beaming thermal emission from hot metallic bull's eyes," *Opt. Express* **18**(5), 4829 (2010).
9. C. Arnold, F. Marquier, M. Garin, F. Pardo, S. Collin, N. Bardou, J.-L. Pelouard, and J.-J. Greffet, "Coherent thermal infrared emission by two-dimensional silicon carbide gratings," *Phys. Rev. B* **86**(3), 035316 (2012).
10. D. Costantini, A. Lefebvre, A.-L. Coutrot, I. Moldovan-Doyen, J.-P. Hugonin, S. Boutami, F. Marquier, H. Benisty, and J.-J. Greffet, "Plasmonic metasurface for directional and frequency-selective thermal emission," *Phys. Rev. Appl.* **4**(1), 014023 (2015).
11. H. Chalabi, A. Alù, and M. L. Brongersma, "Focused thermal emission from a nanostructured SiC Surface," *Phys. Rev. B* **94**(9), 094307 (2016).
12. M. Zhou, E. Khoram, D. Liu, B. Liu, S. Fan, M. L. Povinelli, and Z. Yu, "Self-focused thermal emission and holography realized by mesoscopic thermal emitters," *ACS Photonics* **8**(2), 497–504 (2021).
13. J. Xu, J. Mandal, and A. P. Raman, "Broadband directional control of thermal emission," *Science* **372**(6540), 393–397 (2021).
14. F. Marquier, K. Joulain, J.P. Mulet, R. Carminati, and J.J. Greffet, "Engineering infrared emission properties of silicon in the near field and the far field," *Opt. Commun.* **237**(4-6), 379–388 (2004).
15. Z. Y. Yang, S. Ishii, T. Yokoyama, T. D. Dao, M.-G. Sun, T. Nagao, and K.-P. Chen, "Narrowband wavelength selective thermal emitters confined Tamm plasmon polaritons," *ACS Photonics* **4**(9), 2212–2219 (2017).
16. M. De Zoysa, T. Asano, K. Mochizuki, A. Oskooi, T. Inoue, and S. Noda, "Conversion of broadband to narrowband thermal emission through energy recycling," *Nat. Photon.* **6**(8), 535–539 (2012).
17. L. Dobusch, S. Schuler, V. Perebeinos, and T. Mueller, "Thermal light emission from monolayer MoS₂," *Adv. Mater.* **29**(31), 1701304 (2017).
18. Z. Zhou, E. Sakr, Y. Sun, and P. Bermel, "Solar thermophotovoltaics: reshaping the solar spectrum," *Nanophotonics* **5**(1), 1–21 (2016).
19. M. A. Kats, D. Sharma, J. Lin, P. Genevet, R. Blanchard, Z. Yang, M. Mumtaz Qazilbash, D. N. Basov, S. Ramanathan, and F. Capassol, "Ultra-thin perfect absorber employing a tunable phase change material," *Appl. Phys. Lett.* **101**(22), 221101 (2012).
20. I. Puscasu and W. L. Schaich, "Narrow-band, tunable infrared emissions from arrays of microstrip patches," *Appl. Phys. Lett.* **92**(23), 233102 (2008).
21. X. Liu, T. Tyler, T. Starr, A. F. Starr, N.M. Jokerst, and W. J. Padilla, "Taming the blackbody with infrared metamaterials as selective thermal emitters," *Phys. Rev. Lett.* **107**(4), 045901 (2011).
22. P. Bouchon, C. Koechlin, F. Pardo, R. Haidar, and J.-L. Pelouard, "Wideband omnidirectional infrared absorber with a patchwork of plasmonic nanoantennas," *Opt. Lett.* **37**(6), 1038 (2012).
23. H. T. Miyazaki, T. Kasaya, M. Iwanaga, B. Choi, Y. Sugimoto, and K. Sakoda, "Dual-band infrared metasurface thermal emitter for CO₂ sensing," *Appl. Phys. Lett.* **105**(12), 121107 (2014).
24. E. Rephaeli and S. Fan, "Absorber and emitter for solar thermo-photovoltaic systems to achieve efficiency exceeding the Shockley-Queisser limit," *Opt. Express* **17**(17), 15145 (2009).
25. W. Streyer, S. Law, G. Rooney, T. Jacobs, and D. Wasserman, "Strong absorption and selective emission from engineered metals with dielectric coatings," *Opt. Express* **21**(7), 9113–9122 (2013).
26. C. M. Cornelius and J.P. Dowling, "Modification of Planck blackbody radiation by photonic band-gap structures," *Phys. Rev. A* **59**(6), 4736–4746 (1999).
27. S.-Y. Lin, J. G. Fleming, E. Chow, Jim Bur, K. K. Choi, and A. Goldberg, "Enhancement and suppression of thermal emission by a three-dimensional photonic crystal," *Phys. Rev. B* **62**(4), R2243–R2246 (2000).
28. A. Narayanaswamy and G. Chen, "Thermal emission control with one-dimensional metallodielectric photonic crystals," *Phys. Rev. B* **70**(12), 125101 (2004).
29. M. Garin, T. Trifonov, A. Rodriguez, R. Alcobilla, F. Marquier, C. Arnold, and J.J. Greffet, "Improving selective thermal emission properties of three dimensional macroporous silicon through porosity tuning," *Appl. Phys. Lett.* **93**(8), 081913 (2008).
30. A. Shahsafi, G. Joe, S. Brandt, A. V. Shneidman, N. Stanisic, Y. Xiao, R. Wambold, Z. Yu, J. Salman, J. Aizenberg, and M. A. Kats, "Wide-angle spectrally selective absorbers and thermal emitters based on inverse opals," *ACS Photonics* **6**(11), 2607–2611 (2019).
31. I. Celanovic, D. Perreault, and J. Kassakian, "Resonant-cavity enhanced thermal emission," *Phys. Rev. B* **72**(7), 075127 (2005).
32. C. Fu and Z. M. Zhang, "Thermal radiative properties of metamaterials and other nanostructured materials: a review," *Front. Energy Power Eng. China* **3**(1), 11–26 (2009).
33. Wei Li and Shanhuai Fan, "Nanophotonic control of thermal radiation for energy applications," *Opt. Express* **26**(12), 15995 (2018).
34. D. G. Baranov, Y. Ziao, I. A. Nechepurenko, A. Krasnok, A. Alù, and M. A. Kats, "Nanophotonic engineering of far-field thermal emitters," *Nat. Mater.* **18**(9), 920–930 (2019).
35. S. M. Rytov, Y. A. Kravtsov, and V. I. Tatarskii, *Principles of Statistical Radiophysics* (Springer, 1989).

36. J.-J. Greffet and M. Nieto Vesperinas, "Field theory for the generalized bidirectional reflectivity: derivation of Helmholtz's reciprocity principle and Kirchhoff's law," *J. Opt. Soc. Am. A*, **10**, 2735–2744 (1998).
37. J.-J. Greffet, P. Bouchon, G. Brucoli, E. Sakat, and F. Marquier, "Light emission by nonequilibrium bodies: local Kirchhoff law," *Phys. Rev. X* **8**, 021008 (2018).
38. S. S. Wang and R. Magnusson, "Theory and applications of guided-mode resonance filters," *Appl. Opt.* **32**(14), 2606–2613 (1993).
39. L. Milord, E. Gerelli, C. Jamois, A. Harouri, C. Chevalier, P. Viktorovitch, X. Letartre, and T. Benyattou, "Engineering of slow Bloch modes for optical trapping," *Appl. Phys. Lett.* **106**(12), 121110 (2015).
40. X. Letartre, J. Mouette, J. L. Leclercq, P. Rojo Romeo, C. Seassal, and P. Viktorovitch, "Switching devices with spatial and spectral resolution combining photonic crystal and MOEMS structures," *J. of Lightwave Technol.* **21**(7), 1691–1699 (2003).
41. <https://www.synopsys.com/photonic-solutions/rsoft-photonic-device-tools/passive-device-diffractmod.html>
42. F. Marquier, K. Joulain, J.-P. Mulet, R. Carminati, and J.-J. Greffet, "Coherent spontaneous emission of light by thermal sources," *Phys.Rev.B* **69**(15), 155412 (2004).
43. B. J. Frey, D. B. Leviton, and T. J. Madison, "Temperature dependent refractive index of silicon and germanium," *Proc. SPIE* **6273**, 6272J (2006).
44. S. C. Shen, C. J. Fang, M. Cardona, and L. Genzel, "Far-infrared absorption of pure and hydrogenated a-Ge and a-Si," *Phys. Rev. B* **22**(6), 2913–2919 (1980).